Polymer Testing 128 (2023) 108220

Contents lists available at ScienceDirect

Polymer Testing

journal homepage: www.elsevier.com/locate/polytest

Thermoplastic elastomers based on lactide and caprolactone: The influence of chain microstructure on surface topography and subsequent interaction with cells

Carlos Bello-Álvarez [a], Blanca Atxa Ainz [a], Jone M. Ugartemendia [a], Laura Sebastián [a], Agustin Etxeberria [b], Jose-Ramon Sarasua [a], Ester Zuza [a,**], Aitor Larrañaga [a,*]

[a] Department of Mining-Metallurgy Engineering and Materials Science, POLYMAT, Faculty of Engineering in Bilbao, University of the Basque Country (UPV/EHU), Plaza Ingeniero Torres Quevedo 1, 48013, Bilbao, Spain
[b] Advanced Polymers and Materials: Physics, Chemistry and Technology Department, POLYMAT, University of the Basque Country (UPV/EHU), 20018, Donostia-San Sebastián, Spain

ARTICLE INFO

Keywords:
Thermoplastic elastomers
Chain microstructure
Lactide
Surface topography
Cell interaction

ABSTRACT

Surface biophysical properties of biomaterials, including surface topography and roughness, determine the interaction of a biomaterial with the surrounding cells, tissues and organs once implanted in the human body. Herein, the surface topography of thermoplastic copolymers based on lactide and caprolactone showing elastomeric behaviour was modulated by precisely controlling the chain microstructure (i.e., distribution and length of the repetitive units within the polymeric chain). The synthesized copolymers were subjected to different thermal treatments from the melt, leading to polymeric films with various surface textures and roughness values. Copolymers synthesized with triphenyl bismuth as a catalyst, with a more random distribution of the repetitive units, showed limited crystallization capability. Accordingly, only the copolymer with higher amount of L-lactide (i.e., 80 wt%) subjected to an isothermal treatment from the melt at 70 °C was able to crystallize, and spherulites of around 7 μm were discernible by atomic force microscopy. In contrast, the copolymers synthesized with stannous octoate, which had a more blocky nature, showed axialitic crystalline domains at the submicron-to nanoscale when subjected to an isothermal treatment from the melt at 50 °C, whereas well-defined spherulites of sizes up to 14 μm were obtained at 70 °C. Human fibroblast showed a more elongated morphology when seeded on those samples having higher roughness values and larger spherulites, whereas they had a more spread morphology when seeded on the amorphous, smooth surfaces. As concluded from the present study, by precisely controlling the chain microstructure of the synthesized copolymers, a wide variety of surface topographies can be obtained, which has a clear impact on the way the biomaterial interacts with cells. This opens the possibility to study the influence of surface biophysical properties on more complex cell processes in the future, including inflammatory or foreign body response processes.

Author statement

C.B-Á.: Conceptualization, investigation, writing-original draft; B.A. A.: investigation, writing-review & editing; J.M.U.: conceptualization, writing-original draft; L.S.: investigation, writing-review & editing; A.E.: investigation, methodology, writing-review & editing; J-R. S.: conceptualization, writing-review & editing, funding acquisition; E.Z.: conceptualization, writing-review & editing, supervision; A.L.: writing-original draft, conceptualization, supervision, funding acquisition.

1. Introduction

Tissue engineering relies on the use of scaffolds to repair, regenerate or replace injured tissues in the human body, thus overcoming the inherent drawbacks of more conventional therapies (e.g., autografts, allografts, xenografts) [1]. Ideally, these scaffolds should mimic the intrinsic physical, chemical, mechanical and morphological properties of the extracellular matrix (ECM) where cells reside [2,3]. The surface topography of the scaffolds is of utmost importance in this context, since

* Corresponding author.
** Corresponding author.
E-mail addresses: ester.zuza@ehu.eus (E. Zuza), aitor.larranagae@ehu.eus (A. Larrañaga).

https://doi.org/10.1016/j.polymertesting.2023.108220
Received 15 May 2023; Received in revised form 26 June 2023; Accepted 19 September 2023
Available online 20 September 2023

it determines the interaction between the cells and the biomaterial, being able to modulate the cell differentiation, adhesion, orientation and morphology [4–7]. Moreover, surface topography also influences the foreign body response and accordingly determines the success of the implanted biomaterial for its intended use. Controlling the surface roughness in silicone breast implants [8] or nanopatterning the surface of intracortical microelectrodes with parallel grooves [9] are clear examples of successful strategies to attenuate the inflammatory response after biomaterial implantation.

Copolymers based on L-lactide (L-LA) and ε-caprolactone (ε-CL) have attracted particular attention for the fabrication of biomaterials that interface with soft tissues in the human body, which are characterized by an elastomeric and soft behaviour [10]. By precisely controlling the copolymer composition, synthesis parameters (e.g., reaction time, temperature and catalyst) and processing conditions [11], poly (L-lactide--co-ε-caprolactone) (PLCL) copolymers presenting a variety of mechanical properties (i.e., ranging from a glassy to an elastomeric behaviour), degradation kinetics, shape-memory behaviour and controlled drug-release profiles can be obtained [11,12]. Several studies around the synthesis, characterization and crystal morphology of PLCL have been accordingly conducted, which show the great potential of this family of copolymers [13–15]. The crystallinity behaviour of the PLCL copolymers is vital for tailoring the surface topography of the scaffolds, as different crystallinity degree and crystal morphologies lead to different surface textures and patterns. Thermal treatments, comonomer ratios and chain microstructure (i.e., distribution of repetitive units and number average sequence lengths of the comonomers) determine the supramolecular arrangements, which lead to different properties and crystal morphologies of the copolymers, ranging from spherulites and axialite-like crystal aggregates to amorphous forms [16–18]. Regarding chain microstructure, PLCLs with shorter average length of L-LA unit sequences show a limited crystallization capability, faster degradation rates and higher strain capability and strain recovery values in comparison with PLCLs with larger average lengths (i.e, blockier character) [19]. Additionally, an increasing ε-CL content results in a reduced crystallization capability of PLCL systems, while increasing the elongation at break and strain recovery values and leading to copolymers with different mechanical behaviour, ranging from semi-crystalline plastic--like to elastomeric [20].

Chain microstructure can be controlled by adjusting the conditions of the synthesis process, the employed catalysts and the rates of incorporation of the comonomers [19]. In the case of PLCLs, there is a large difference in the reactivity of L-LA and ε-CL units in the ring opening copolymerization process, which naturally favours the formation of blocky chain microstructures [21,22]. Adjusting the relationship between reactivities, favouring transesterification reactions or controlling the polymerization temperature and reaction time [19] are common strategies to modulate the randomness character of the resulting copolymers. The use of different catalysts/initiators has also been studied as a strategy to tune the chain microstructure of PLCL copolymers [14,15,22,23]. Stannous octoate ($SnOct_2$) is the most commonly used catalyst for ring-opening polymerization due to its good performance, with high conversion and reaction rates and the possibility to obtain (co) polymers with high molecular weights. This catalyst has been reported to lead to blocky PLCLs [14,19]. Bismuth salts (e.g., $BiCl_3$, Bi_2O_3, diphenyl bismuth bromide [24,25]) used in different polymerizations, on the other hand, have been successfully employed to synthesize PLCL systems with more random nature [19]. Triphenyl bismuth (Ph_3Bi), in particular, has been used in the synthesis of other random copolyesters, namely, poly (L-lactide-co-δ-valerolactone) and poly (ethylene brassylate-co-ε-caprolactone) [26,27].

In the present study, with the aim of studying the effect of chain microstructures on the surface topography and mechanical properties of the synthesized copolymers, a variety of PLCLs were synthesized by ring-opening polymerization. Controlling the comonomer mass feed ratios and the catalyst/initiator (i.e., $SnOct_2$ or Ph_3Bi), PLCL copolymers showing different compositions and chain microstructures were obtained. These copolymers were subjected to isothermal treatments to control crystallinity degree (determined by means of differential scanning calorimetry) and crystal morphology (assessed by atomic force microscopy). Finally, human pulmonary fibroblasts (i.e., MRC-5 cells) were seeded on PLCLs showing different surface topographies to study the impact of surface topography on cell morphology.

2. Materials and methods

2.1. Materials

ε-Caprolactone (ε-CL) monomer and Stannous octoate ($SnOct_2$) catalyst were supplied by Merk KGaA (Germany), while L-Lactide (L-LA) monomer was provided by Corbion (The Netherlands). Triphenyl Bismuth (Ph_3Bi) catalyst was obtained from Gelest (USA). Dichloromethane and methanol were supplied by Labbox (Spain). Dulbecco's Modified Eagle Medium (DMEM), Hanks' Balanced Salt Solution (HBSS), Penicillin/Streptomycin (P/S), Foetal Bovine Serum (FBS) and rhodamine-phalloidin (Rd/Ph) were supplied by Fisher Scientific (Spain). Primary antibody Vinculin (ab129002) was supplied by Abcam (UK). Secondary antibody AlexaFluor 488 donkey anti-rabbit IgG and 16% Formaldehyde (PFA) solution were supplied by Thermo Fisher Scientific (USA). Phosphate-buffered saline (PBS), Triton X-100, Tween 20 and Fluoroshield with DAPI were supplied by Sigma Aldrich (Spain). Chloroform was supplied by PanReac (Spain).

2.2. Synthesis

Four different PLCL copolymers were synthetized following our previously reported protocol [28]. Briefly, copolymers based on L-LA and ε-CL were synthesized in bulk by one-pot-one-step ring-opening polymerization (ROP) with two different feed mass ratios of 80 wt% L-LA – 20 wt% ε-CL and 70 wt% L-LA – 30 wt% ε-CL. Predetermined amounts of the comonomers were placed into a round bottom flask and immersed into a controlled temperature oil bath at 140 °C until melting. To ensure an inert atmosphere, a nitrogen stream was initiated under the surface of the melt for 15 min. Subsequently, the catalyst (Ph_3Bi or $SnOct_2$) was added at a 1000:1 comonomers:catalyst molar ratio while stirring. After 24 h of reaction, the resulting product was dissolved in dichloromethane and precipitated in an excess of methanol to remove impurities and those monomers that had not reacted. Finally, the product was dried at room temperature and then dried at 100 °C for 1 h to ensure the complete elimination of remaining solvents.

2.3. Differential scanning calorimetry (DSC)

The thermal properties of the synthesized copolymers were analysed by Q200-Differential Scanning Calorimeter (TA Instruments). Samples weighing between 5 and 10 mg were encapsulated in hermetic aluminium pans to study the glass transition temperature (T_g), melting temperature (T_m) and melting enthalpy (ΔH_m). Two scans were performed. Both scans were carried out from −40 to 200 °C at 20 °C min^{-1}.

2.4. Gel permeation chromatography (GPC)

Samples were prepared at a concentration of 10 mg mL^{-1} using chloroform as solvent. Then, the molecular weight (M_w) and distribution of the synthesized copolymers were determined in a Waters 1515 GPC device equipped with two Styragel columns (10^2 - 10^4 Å).

2.5. Nuclear magnetic resonance (NMR)

Proton and carbon nuclear magnetic resonance (^1H NMR and ^{13}C NMR) spectra were acquired in a Bruker Avance DPX 300 at 300.16 MHz and 75.5 MHz of resonance frequency respectively, using 5 mm O.D.

sample tubes, following the previously optimized protocol [11].

Using the tables of structural determination from Prestch et al. [29], the different signals were assigned. By averaging the values of molar contents and the LA-CL dyad relative molar fractions that were obtained by means of ^{1}H and ^{13}C NMR spectroscopy, the copolymer composition data, average sequence lengths, and randomness character were calculated. The number average sequence lengths (l_i), the Bernoullian random number average sequence lengths $(l_i)_{random}$ and the randomness character (R) were obtained using equations (eq. (1)) to (eq. (4)):

$$l_{LA} = \frac{(LA-LA)+\frac{1}{2}(LA-CL)}{\frac{1}{2}(LA-CL)} = \frac{2(LA)}{(LA-CL)} \quad (1)$$

$$l_{CL} = \frac{(CL-CL)+\frac{1}{2}(LA-CL)}{\frac{1}{2}(LA-CL)} = \frac{2(CL)}{(LA-CL)} \quad (2)$$

$$(l_{LA})_{random} = \frac{1}{(CL)} \; ; (l_{CL})_{random} = \frac{1}{(LA)} \quad (3)$$

$$R = \frac{(l_{LA})_{random}}{l_{LA}} = \frac{(l_{CL})_{random}}{l_{CL}} \quad (4)$$

where (LA) and (CL) are the lactide and caprolactone molar fractions, and (LA-CL), (LA-LA) and (CL-CL) are the LA-CL, LA-LA and CL-CL average dyad relative molar fractions, respectively.

2.6. Thermal treatments

The synthesized copolymers were subjected to three different thermal treatments within the Q200-Differential Scanning Calorimeter (TA Instruments): quenching treatment and isothermal crystallization treatments from the melt at 50 °C and 70 °C. Prior to these treatments, the thermal history of the samples was erased in a first scan by increasing the temperature to 200 °C. Afterwards, the isothermal crystallizations were carried out from the melt, quenching to the specific temperature at a rate of 20 °C min^{-1} and maintaining at the selected temperature (i.e., 50 or 70 °C) for 24 h. After the isothermal crystallization, the samples were rapidly quenched within the DSC to −40 °C and subjected to a second scan from −40 to 200 °C at a rate of 20 °C min^{-1}. For the quenching treatments, a similar process was followed, first increasing the temperature to 200 °C, rapidly quenching to −40 °C and performing a second scan up to 200 °C at 20 °C min^{-1}. The crystallinity degree (χ) of the samples was calculated based on the amount of lactide in the copolymer (determined from NMR analysis) and the enthalpy of fusion of the polylactide crystal ($\Delta H_m^0 = 106$ J g^{-1}) [30].

2.7. Atomic force microscopy (AFM)

The surface of the copolymers subjected to different thermal treatments (i.e., quenching and isothermal treatments from the melt at 50 and 70 °C) was analysed using a Nanoscope V Multimode AFM (Bruker). The images were obtained in PeakForce Tapping mode and employing a scanasyst-air silicon tip on nitride lever type tip, with a tip radius of 2 nm, a resonance frequency between 45 and 95 kHz and spring constant of 0.2–0.8 N m^{-1}. Polymeric films of 40–70 μm were obtained by solvent casting. Solutions of concentration 5 w/v% (weight/volume ratio) in dichloromethane were poured into petri dishes. Samples were dried under the fume hood for 24 h at room temperature and then were vacuum-dried for another 24 h. Once the films were obtained, they were thermally treated. Firstly, the resulting samples were melted at 200 °C and held at this temperature for 2 min. Then, for isothermal treatments, the samples were cooled from the melt to the selected crystallization temperature (50 or 70 °C) and kept for 24 h. Finally, the films were rapidly cooled to room temperature. For the quenching treatment, the temperature of the films was rapidly lowered from 200 to −20 °C. Finally, the films were placed on glass disks and images of the topography (height image) and peak force error were acquired in different areas and various scan sizes. To obtain a comprehensive view of the morphology of the samples, several locations were scanned for each sample, progressively decreasing the scan size to allow the observation of the smaller structures.

Images were then analysed by Nanoscope Analysis software. The size of crystalline formations was measured analysing the cross-sections of the height images. The roughness of the surface topology feature of PLCL films were quantified by the mean roughness (R_a).

2.8. Tensile test

To study the mechanical properties of the resulting materials, the specimens were prepared by compression moulding, as previously described [10]. First, a predetermined amount of copolymer was melted at 180 °C and, subsequently, 250 bar were applied for 45 s. The samples were then rapidly quenched within the compression moulding machine. In this way, films of 250 μm thickness were obtained for mechanical evaluation. The tensile tests were carried out with an Instron 5565 testing machine at a crosshead displacement rate of 10 mm min^{-1} at room temperature (21 ± 2 °C). All properties were determined as a mean value of at least four determinations, using samples of 100 mm in length and 10 mm wide with an average thickness of 250 μm.

2.9. Cell adhesion study and immunostaining

MRC-5 cells (ATCC CCL-171) were cultured in DMEM supplemented with 10% FBS and 1% P/S and incubated in a humidified atmosphere (5% CO_2, 95% relative humidity) at 37 °C. Samples of 5 × 5 mm from the selected systems showing different surfaces textures (PLCL 7030 Sn iso T = 70 °C; PLCL 8020 Bi iso T = 70 °C; PLCL 8020 Sn iso T = 50 °C and PLCL 7030 Sn quenched) were placed in a culture plate, extensively washed with ethanol and subsequently washed with PBS before being air dried inside the biosafety cabinet. Then, samples were placed under ultraviolet light for 15 min to ensure sterilization. For this study, cells were seeded at a density of 2000 cells/sample. After 24 h of incubation, the culture media was aspirated and cells were washed twice with PBS before fixation with 4% PFA for 5 min. Then the PFA solution was removed and samples were washed again twice with PBS. A solution of 0.5% Triton X-100 in PBS was added and kept under slight agitation for 7 min to permeabilize the cell membrane. The solution was removed and the samples were washed again with PBS under slight agitation for 3 min, three times. A solution (1% BSA, 0.1% Tween 20 and 1:100 primary antibody) was prepared and samples were incubated with that solution in a humid chamber overnight at 4 °C. Then, the samples were washed with 0.05% Tween 20 in PBS three times and incubated with a solution containing the secondary antibody (1:200), Rd/Ph (1:100) and 1% BSA in 0.1% Tween 20 in PBS for 2.5 h in the humid chamber at 4 °C. The solution was subsequently aspirated and the samples were washed with a 0.05% Tween 20 in PBS for 7 min twice under agitation. Finally, they were washed with PBS twice for 7 min under agitation and were kept in fresh PBS before observing under fluorescence microscope. Nuclei staining with DAPI was carried out directly on the samples by adding a drop of mounting medium before observing them under the microscope (Nikon Eclipse Ts2).

3. Results and discussion

3.1. Characterization of synthesized copolymers

In this work, four different PLCLs showing different comonomer ratios and chain microstructures were synthesized by ring-opening polymerization (Table 1). The M_w achieved with this reaction was slightly higher for those copolymers synthesized with Ph_3Bi (PLCL 8020 Bi: 139,600 g mol^{-1} and PLCL 7030 Bi: 121,400 g mol^{-1}) than those with $SnOct_2$ (PLCL 8020 Sn: 101,600 g mol^{-1} and PLCL 7030 Sn: 112,300 g

Table 1
Characterization of the synthesized copolymers.

	PLCL 8020 Bi	PLCL 8020 Sn	PLCL 7030 Bi	PLCL 7030 Sn
M_w (g mol^{-1})	139,600	101,600	121,400	112,300
T_g (°C) (2nd scan)	28.2	27.3	14.0	18.3
T_m (°C) (1st scan)	105.5	144.6	127.6	135.0
ΔH_m (J g^{-1}) (1st scan)	13.3	25.4	1.5	21.0
χ (%)	15.9	30.0	2.0	28.6
l_{LA}	3.65	5.38	2.45	4.31
l_{CL}	1.24	1.70	1.28	2.42
R	1.08	0.77	1.19	0.65
% (weight) LA	78.9	80.0	70.7	69.3
% (weight) CL	21.1	20.0	29.3	30.7

mol^{-1}) [31]. As expected from the glass transition temperature values of the homopolymers (i.e., T_g of PLLA around 60 °C and for PCL of −60 °C [32]), a higher T_g was observed in those copolymers with more LA content (PLCL 8020 Bi: 28.2 °C and PLCL 8020 Sn: 27.3 °C) than in those with a lower LA content (PLCL 7030 Bi: 14.0 °C and PLCL 7030 Sn: 18.3 °C) (Fig. 1S). On the other hand, T_m and crystallinity degree (χ) strongly depended on the used catalyst and derived chain microstructure. The use of Ph_3Bi as a catalyst resulted in copolymers with lower T_m and χ (PLCL 8020 Bi: $T_m = 105.5$ °C; $\chi = 15.9\%$ and PLCL 7030 Bi $T_m = 127.6$ °C; $\chi = 2.0\%$) in comparison to the copolymers synthesized using $SnOct_2$ (PLCL 8020 Sn: $T_m = 144.6$ °C; $\chi = 30.0\%$ and PLCL 7030 Sn $T_m = 135.0$ °C; $\chi = 28.6\%$).

Regarding the chain microstructure parameters, calculated by averaging the results obtained from ^{1}H and ^{13}C NMR spectroscopy (Fig. 2S–9S), the use of Ph_3Bi as catalyst favoured the formation of LA-CL dyads and alternating LA-CL-LA triads, shortening the repeat unit length values of LA (l_{LA}) and CL (l_{CL}) and leading to copolymers displaying a random character (R value close to 1). This suggests the presence of alternating monomer sequences (-LA-CL-LA-CL-LA-CL-) in the copolymer chains, explained by the transesterification reactions in the synthesis process, which lead to a shortening of the blocks in the polymer chains [33]. This effect is especially remarkable in the case of the 70:30 monomer feed ratio. More ε-CL was available during the synthesis process, allowing the easier formation of these alternating sequences, which also explains the higher R value. On the other hand, the systems synthesized using $SnOct_2$ showed a blockier (but still random distribution) tendency with lower values of R, and longer repeat unit lengths.

Considering the results obtained by NMR and DSC, it can be concluded that a higher R and a shorter l_{LA} (copolymers synthesized with Ph_3Bi) limit the capability of crystallization of the lactide units, causing the T_m to be lower and reducing the crystallinity degree greatly, which is evidenced in the first DSC scan (Fig. 1S). In the case of the PLCL 7030 Bi, the crystallinity degree of the nascent copolymer is negligible. For the copolymers synthesized using $SnOct_2$, a much higher crystallinity degree (χ) was observed, with fractions around 30% in both cases. Both the crystallinity fraction and the T_m were slightly higher in the case of the PLCL 8020 Sn system. This could be explained by both a higher amount of crystallisable L-lactide units and the presence of longer repetitive units. It is worth mentioning that the T_g signals present a larger ΔC_p in the PLCLs with a lower crystallinity degree, as a higher proportion of the copolymer undergoes the glass transition in these cases. In the second scan (Fig. 1S), all the PLCLs showed a homogeneous amorphous phase except the PLCL 8020 Sn, which showed a minimal melting peak.

3.2. Thermal treatments

The synthesized copolymers were subjected to three thermal treatments (i.e., quenching and isothermal treatments from the melt at either 70 or 50 °C) within the DSC to analyse their crystallization behaviour (Table 2 and Fig. 10S). As expected, the crystallization capability of the copolymers increases with the length of the LA repeat sequences (l_{LA}). Accordingly, the calculated l_{LA} value for the PLCL 7030 Bi (i.e., $l_{LA} = 2.45$) is not enough to produce crystalline domains under the studied conditions. In contrast, the calculated l_{LA} value for the PLCL 8020 Bi (i.e., $l_{LA} = 3.65$) is sufficient to form crystalline domains when subjected to an isothermal treatment at 70 °C for 24 h, showing a T_m of 108.6 °C. The copolymers synthesized with $SnOct_2$ as catalyst, thanks to their blockier character and subsequent longer l_{LA} (i.e., $l_{LA} > 4$), were prone to form crystalline domains after being subjected to isothermal treatments from the melt with melting points centred at around 139 °C. In any case, the T_m values of these copolymers are significantly lower than the T_m of PLLA homopolymer ($T_m = 170$–183 °C) [28]. These differences could be

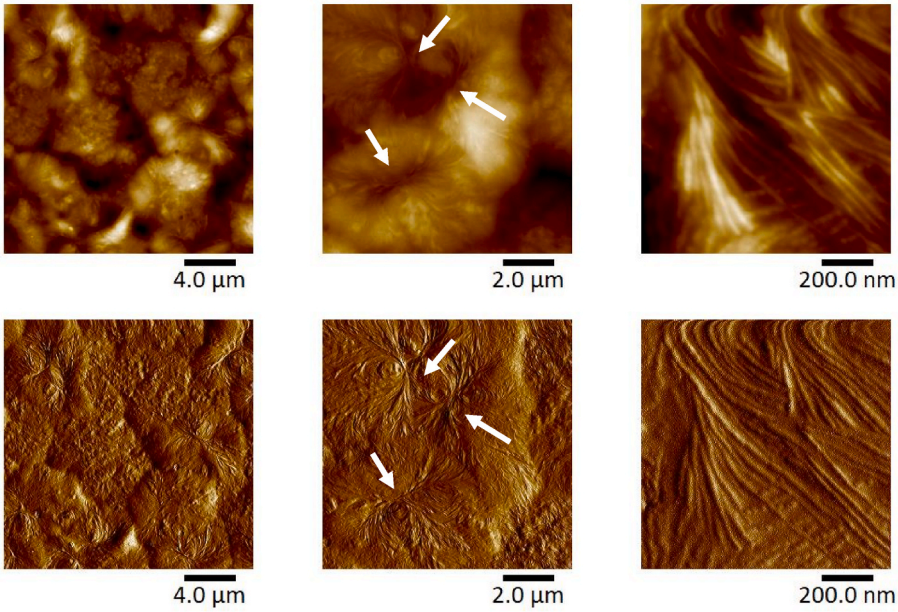

Fig. 1. Atomic force microscopy height image (top) and peak force error image (bottom) of PLCL 8020 Bi isothermally crystallized at 70 °C. White arrows highlight nucleation points.

Table 2
Thermal properties of quenched and isothermally crystallized poly (L-lactide-co-ε-caprolactone) (PLCL) for 24 h. T_c: isothermal crystallization temperature; T_g: glass transition temperature; T_m: melting temperature; ΔH_m: melting enthalpy; χ: crystallinity degree.

	T_c (°C)	T_g 1 (°C)	T_g 2 (°C)	T_m (°C)	ΔH_m (J/g)	χ (%)
PLCL 8020 Bi	quenched	28.2	–	–	–	0.0
	50	31.3	–	–	–	0.0
	70	25.2	–	108.6	16.5	19.8
PLCL 8020 Sn	quenched	27.3	–	–	–	0.0
	50	13.3	69.2	139.4	23.2	27.4
	70	10.6	84.7	138.1	24.0	28.3
PLCL 7030 Bi	quenched	14.0	–	–	–	0.0
	50	16.1	–	–	–	0.0
	70	15.4	–	–	–	0.0
PLCL 7030 Sn	quenched	18.3	–	–	–	0.0
	50	3.4	70.4	139.7	16.7	22.8
	70	2.1	86.2	139.9	15.8	21.5

attributed to the decrease of l_{LA} (Table 1) promoted by the presence of ε-CL repetitive units [16]. Contrarily to the melting peaks commonly observed for pure PLLA, which are relatively well-defined unimodal peaks [34], double endothermic peaks were observed in our synthesized copolymers (Fig. 10S). This can be explained by a melt-recrystallization phenomenon. Low perfection crystals are melted to recrystallize with higher perfection and melt again at a higher temperature. This could be due to the existence of crystals with different morphologies of lamellae with variable thicknesses or by there being an intermediate constrained phase between the crystalline and the amorphous phases [35]. As expected, when these copolymers were rapidly quenched from the melt, they showed a completely amorphous character.

Regarding the variation of the crystallinity degree with the selected isothermal crystallization temperatures, a clear trend was not observed. Those copolymers synthesized with $SnOct_2$ showed very similar crystallinity degree values irrespective of the selected isothermal crystallization temperature (i.e., PLCL 8020 Sn: 27.4 and 28.3% at 50 and 70 °C, respectively; PLCL 7030 Sn: 22.8 and 21.5% at 50 and 70 °C, respectively). For Ph_3Bi systems, PLCL acts as a single-phase amorphous copolymer showing a single hybrid T_g located between the T_g values of the pure homopolymers. However, for those copolymers synthesized with $SnOct_2$, two T_g were registered. The lower T_g is associated to the hybrid amorphous miscible LA-CL phase, composed mostly of ε-CL units and the higher T_g suggests the presence of amorphous LA domains which are phase separated and may be constrained between the crystalline regions [36].

3.3. Atomic force microscopy (AFM)

The synthesized PLCLs showed distinct topographies depending on the used catalyst (Ph_3Bi or $SnOct_2$) and subsequent heat treatment (quenching, isothermal crystallization at 50 and 70 °C), from very smooth surfaces for amorphous samples to rougher ones for crystallized samples.

In line with the DSC observations, those PLCLs synthesized with Ph_3Bi showed amorphous structures, except the PLCL 8020 Bi isothermally treated at 70 °C. The rest of the samples showed a smooth surface ($R_a < 2$ nm) with no discernible crystalline domains (see Supplementary Fig. 11S). The sample treated at 70 °C presented spherulitic morphology with average size spherulites of 7 μm. Nucleation points (white arrows) around which lamellae branch out and spherulites grow are easily distinguished in Fig. 1.

Regarding the PLCLs synthesized with $SnOct_2$, both compositions, 8020 and 7030, presented an amorphous nature after quenching from the melt, similar to those displayed in Fig. 11S. However, both copolymers showed crystallization capability after isothermal heat treatment at specified temperatures. Interestingly, the final crystal structure varies depending on the degree of undercooling and consequently, a variety of topographic textures were obtained in terms of shape and roughness. This change in surface topology feature of the substrates following the different crystallization strategies could influence not only the mechanical properties, but also the interaction of the biomaterial with the surrounding cells and tissues once implanted.

Isothermal treatment at 50 °C resulted in a small axialite-like crystalline structure for both copolymers, PLCL 8020 Sn and PLCL 7030 Sn (Fig. 2). The presence of numerous nucleation points at low crystallization temperatures resulted in the early impingement of crystals that cannot further grow resulting in a low roughness lamellar pattern. The average size of these lamellar crystalline structures was calculated to be 285–300 nm and the mean roughness values (R_a) 8.11 nm and 14.3 nm for PLCL 8020 Sn and PLCL 7030 Sn, respectively.

The isothermal treatment at 70 °C led to clearly defined spherulitic crystalline structures for both copolymers (Fig. 3). The observed spherulites showed a typical crystalline structure of the poly (L-lactide) homopolymer where edge-on and flat-on structures, numbered in Fig. 3 as 1 and 2 respectively, are easily identified in the high-magnification AFM images [37]. Although there is a slight difference in the average size of the spherulites for both copolymers, 12 μm for PLCL 8020 Sn and 14 μm for PLCL 7030 Sn, bigger spherulites could be observed for the latter one, measuring up to 18 μm. The fact that PLCL 7030 Sn forms larger crystals even with less lactide content and shorter lactide building blocks (l_{LA} for PLCL 7030 Sn = 4.31 vs. l_{LA} for PLCL 8020 Sn = 5.38), is attributable to two effects: (1) its more multiblock macromolecular chain microstructure (R for PLCL 7030 Sn = 0.65 vs. R for PLCL 8020 Sn = 0.77), which might help in the crystallization process and (2) the crystallization kinetics. Both copolymers have different glass and melting temperature (see Table 1) and, therefore, the 70 °C crystallization temperature (T_c) involves different levels of undercooling ($\Delta T = T_m - T_c$) for each. Smaller undercooling, as in the case of the PLCL 7030 Sn, implies the formation of less nucleation points, enabling the spherulites to grow bigger before they collide with each other.

The values of surface roughness as a function of heat treatment allows us to directly differentiate the effect of crystallization process on PLCLs surface topology feature. Table 3 summarizes the morphologies, crystal sizes and mean roughness (R_a) of all the samples. Results revealed a remarkable difference in the roughness of the samples with spherulitic morphologies and those with either amorphous or lamellar morphologies. The presence of spherulitic morphologies, especially the PLCL 8020 Sn and PLCL 7030 Sn systems treated isothermally at 70 °C, have microcavities between the spherulites and characteristic topographies, leading to mean roughness values greater than 110 nm. However, at the same crystallization conditions, the PLCL 8020 Bi samples showed lower mean roughness value, around 39 nm. The crystalline behavior of these copolymers is very conditioned by their L-lactide average sequence length (l_{LA}) and randomness character (R). Shorter l_{LA} and higher randomness character, as in the case of the PLCL 8020 Bi, involve smaller and less regular/uniform/perfect spherulites as shown in Fig. 1, resulting in less rough surfaces.

3.4. Mechanical properties

The mechanical properties of the synthesized copolymers were determined by tensile test at room temperature (21 ± 2 °C) (Fig. 4), where three well differentiated behaviours are discernible. Those samples with a lower content in LA (i.e., PLCL 7030 Sn and PLCL 7030 Bi) presented an elastomeric behaviour, characterized by a low stiffness and a high strain recovery capacity after break (Table 4). However, important differences were observed in the mechanical behaviour depending on the selected catalyst (i.e., $SnOct_2$ vs. Ph_3Bi). PLCL 7030 Bi showed a low secant modulus at 2% of 6.5 MPa, a strain recovery of 88.8% and an elongation at break of 589.4%. In contrast, although the PLCL 7030 Sn also showed an elastomeric behaviour, with a low secant modulus at 2% of 18.9 MPa, a strain recovery of 83.5% and an elongation at break of

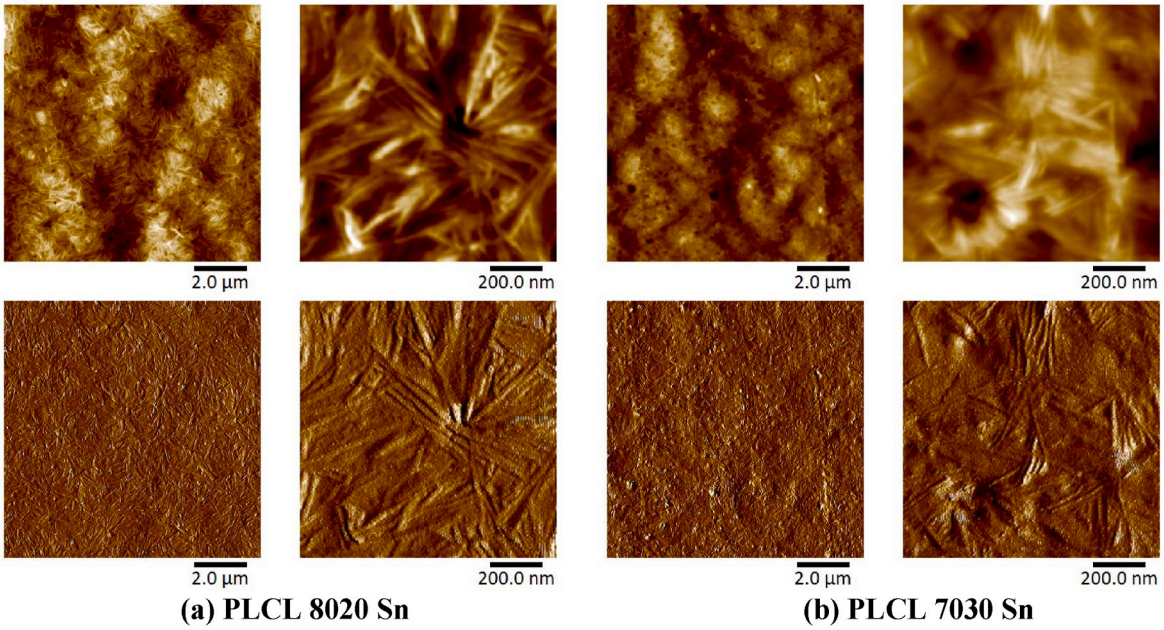

Fig. 2. Atomic force microscopy height images (top) and peak force error images (bottom) of (a) PLCL 8020 Sn and (b) PLCL 7030 Sn isothermally crystallized at 50 °C.

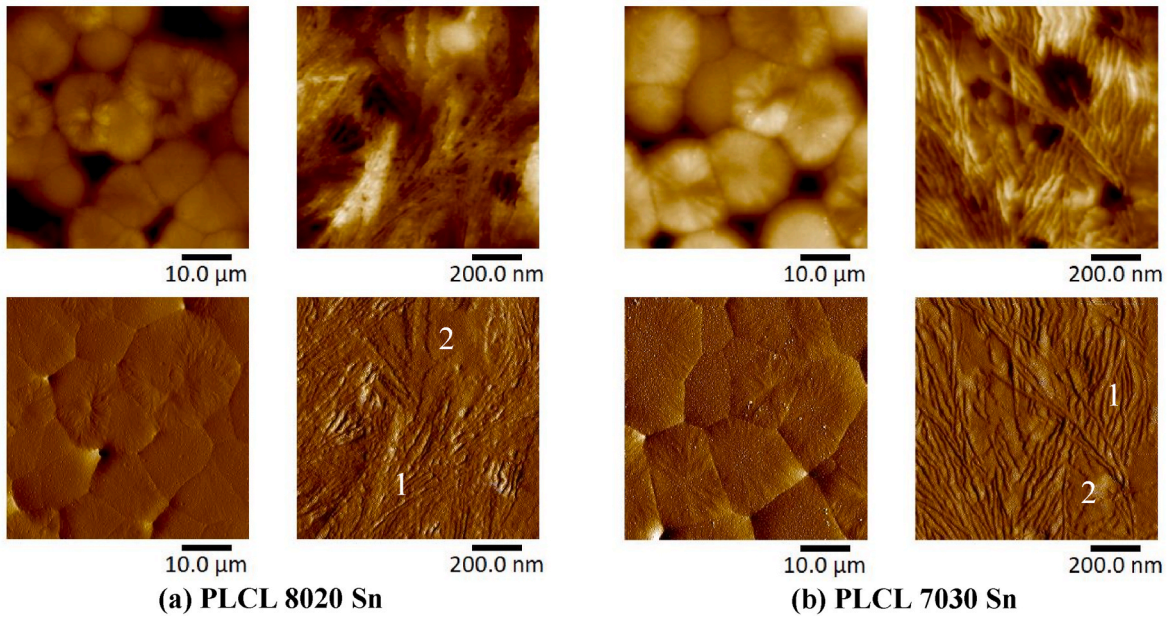

Fig. 3. Atomic force microscopy height images (top) and peak force error images (bottom) of (a) PLCL 8020 Sn and (b) PLCL 7030 Sn isothermally crystallized at 70 °C. [Number 1 and 2 pointed edge-on and flat-on crystalline structures, respectively].

268.6%, it also presented the strain-hardening phenomena at high deformations, reaching an ultimate tensile strength of 16.5 MPa. On the other hand, the copolymers with higher content in LA (i.e., PLCL 8020 Sn and PLCL 8020 Bi) showed a plastic behaviour, characterized by a well-defined yield point, a lower elongation at break (186.8% for PLCL 8020 Sn and 205.0% for PLCL 8020 Bi) and strain recovery of 32.5% for PLCL 8020 Sn and 41.9% for PLCL 8020 Bi. Also, these copolymers exhibited the strain-hardening phenomena at high deformations, which can be associated to the chain alignment at high deformations.

In general terms, it can be concluded that the more random distribution of the repetitive units obtained with the catalyst based on Ph_3Bi, results in softer copolymers with lower stiffness, higher elongation at break and higher strain recovery after break. These behaviours are in line with the results obtained in DSC (Table 2).

3.5. Interaction of human fibroblasts with various polymeric topographies

The surface topography of a biomaterial is of utmost importance in determining the fate of the surrounding cells, tissues and organs when the biomaterial is implanted in the human body. As demonstrated in the present study, by controlling the chain microstructure of L-lactide and ε-caprolactone based copolymers, a plethora of surface topographies can be developed via several thermal treatments from the melt, which will presumably determine the interaction of cells with the biomaterial.

Table 3
Morphologies and roughness of quenched and isothermally crystallized PLCL.

	Treatment	Morphology	Size	R_a (nm)
PLCL 8020 Bi	quenching	amorphous	–	0.223
	iso. 50 °C	amorphous	–	1.76
	iso. 70 °C	spherulitic	7 μm	39.20
PLCL 8020 Sn	quenching	amorphous	–	0.882
	iso. 50 °C	lamellar/axialitic	300 × 32 nm/800 nm	8.11
	iso. 70 °C	spherulitic	12 μm	136
PLCL 7030 Bi	quenching	amorphous	–	0.215
	iso. 50 °C	amorphous	–	0.302
	iso. 70 °C	amorphous	–	0.203
PLCL 7030 Sn	quenching	amorphous	–	1.70
	iso. 50 °C	lamellar	285 nm × 25 nm	14.30
	iso. 70 °C	spherulitic	14 μm	110

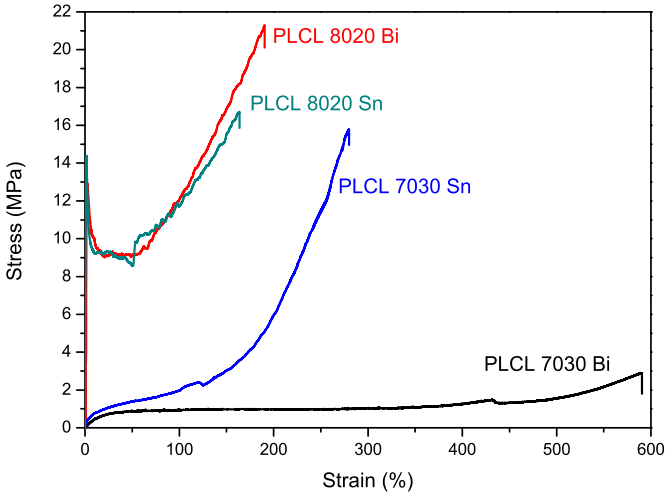

Fig. 4. Stress-strain curves of the synthesized PLCL copolymers.

Herein, the interaction of MRC-5 cells (human fibroblasts) with different surface topographies was evaluated as a preliminary *in vitro* study to gain more insights about the influence of surface topography on cell behaviour. Four PLCL samples displaying different surface topographies were selected for this purpose: i) PLCL 7030 Sn subjected to an isothermal treatment at 70 °C, ii) PLCL 8020 Bi subjected to an isothermal treatment at 70 °C, iii) PLCL 8020 Sn subjected to an isothermal treatment at 50 °C and iv) PLCL 7030 Sn subjected to a rapid quenching from the melt. The selected samples had roughness (R_a) values ranging from 1.7 to 110 nm, crystallinity degrees ranging from 0 to 27.4% and different crystal morphologies (spherulitic, lamellar/axialitic), thus covering a wide range of surface topographies. As observed in the obtained micrographs (Fig. 5a-d), cells had a more elongated morphology in the PLCL 7030 Sn sample subjected to an isothermal treatment at 70 °C (Fig. 5a). This sample, as previously concluded from the AFM evaluation, had a spherulitic structure with spherulites of ~14 μm. In contrast, for the PLCL 7030 Sn sample subjected to a rapid quenching, cells showed a completely different shape, characterized by a more spread morphology. The surface of this sample was smooth and showed the lowest R_a value among the studied samples (R_a of 1.7 nm). These differences observed under the fluorescent microscope were further supported by quantitative values of nuclei area and aspect ratio (Fig. 5e and f). Statistically significant differences ($p < 0.05$) were observed in these two parameters between PLCL 7030 Sn sample subjected to an isothermal treatment at 70 °C or rapidly quenched from the melt. Accordingly, the nuclei area increased from 412.2 ± 8.4 μm^2 in the isothermally crystallized copolymer to 571.1 ± 11.3 μm^2 in the rapidly quenched sample. The aspect ratio (length/width) decreased from 1.83 ± 0.03 in the isothermally crystallized copolymer to 1.72 ± 0.02 in the rapidly quenched sample, thus confirming the conclusions drawn from the micrographs. A similar behaviour has been reported in bibliography with human articular chondrocytes [38]. In the reported study, human chondrocytes were seeded on the surface of PLLA with increasing sizes of spherulites. Those cells seeded on the PLLA sample showing largest spherulites (30–50 μm) display a more elongated morphology and preferred orientation, similar to the so-called contact guidance observed in nanostructured topographies. The PLCL 8020 Bi subjected to an isothermal treatment at 70 °C shows an intermediate behaviour between the aforementioned PLCL 7030 Sn samples. In comparison to the PLCL 7030 Sn isothermally crystallized, the PLCL 8020 Bi sample shows lower R_a value (110 vs. 39.2 nm), lower crystallinity degree (21.5 vs 19.8%) and smaller spherulites (14 vs 7 μm). Statistically significant differences ($p < 0.05$) were observed in the nuclei area (412.2 ± 8.4 μm^2 for the PLCL 7030 Sn vs. 490.3 ± 9.5 μm^2 for the PLCL8020 Bi) of the cells seeded in these two samples. In the case of nuclei aspect ratio, although not statistically significant, a slight decrease was observed (from 1.83 ± 0.03 for the PLCL 7030 Sn to 1.81 ± 0.03 for the PLCL 8020 Bi), suggesting again that larger spherulites promote a more elongated shape of the seeded cells. Finally, the PLCL 8020 Sn sample subjected to an isothermal treatment at 50 °C was analysed. This sample, contrarily to the previously analysed ones, had a lamellar/axialitic crystal morphology and a R_a value of 8.1 nm. Although no significant differences were observed with respect to the PLCL 8020 Bi sample subjected to an isothermal treatment at 70 °C, cells appeared to be more elongated in the PLCL 8020 Sn sample isothermally crystallized at 50 °C (nuclei area was 490.3 ± 9.5 μm^2 for the PLCL8020 Bi and 466.3 ± 12.2 μm^2 for the PLCL 8020 Sn; aspect ratio was 1.81 ± 0.03 for the PLCL 8020 Bi and 1.82 ± 0.02 for the PLCL 8020 Sn). These results suggest that, not only the roughness of the surface, but also the crystal morphology of the sample may influence the cell fate.

Despite we focused our discussion on the influence of surface topographies on cell behaviour, it has to be considered that other physical properties (e.g., mechanical properties, different polarity/hydrophobic nature of the substrate, etc.) are also important in determining the interaction of cells with a biomaterial. Besides, it has to be considered that the crystallization process of the copolymers studied herein can result in the localization of PCL units due to the phase separation (as demonstrated by the DSC thermograms where two glass transition temperatures were observed in those samples synthesized with $SnOct_2$), giving rise to the presence of PCL-rich domains on the surface of the sample. These domains may present different polarity/hydrophobic nature, thus influencing cell interaction. Regarding the hydrophilicity/hydrophobicity of the surface, we determined that semicrystalline PCL, semicrystalline PLLA and amorphous PLLA showed virtually the same water contact angle values (Table 1S) despite their different chemical structure in the repeating unit and different degrees of crystallinity

Table 4
Mechanical properties of the synthesized PLCL copolymers.

	Young's modulus (MPa)	Secant modulus at 2% (MPa)	Ultimate Tensile Strength (MPa)	Elongation at break (%)	Strain recovery (%)
PLCL 8020 Bi	1795.2 ± 206.2	693.4 ± 63.7	23.1 ± 2.1	205.0 ± 18.8	41.9
PLCL 8020 Sn	2667.3 ± 66.7	714.9 ± 51.4	17.9 ± 1.8	186.8 ± 21.0	32.5
PLCL 7030 Bi	–	6.5 ± 1.8	2.0 ± 0.2	589.4 ± 26.3	88.8
PLCL 7030 Sn	–	18.9 ± 3.1	16.5 ± 0.4	268.6 ± 29.2	83.5

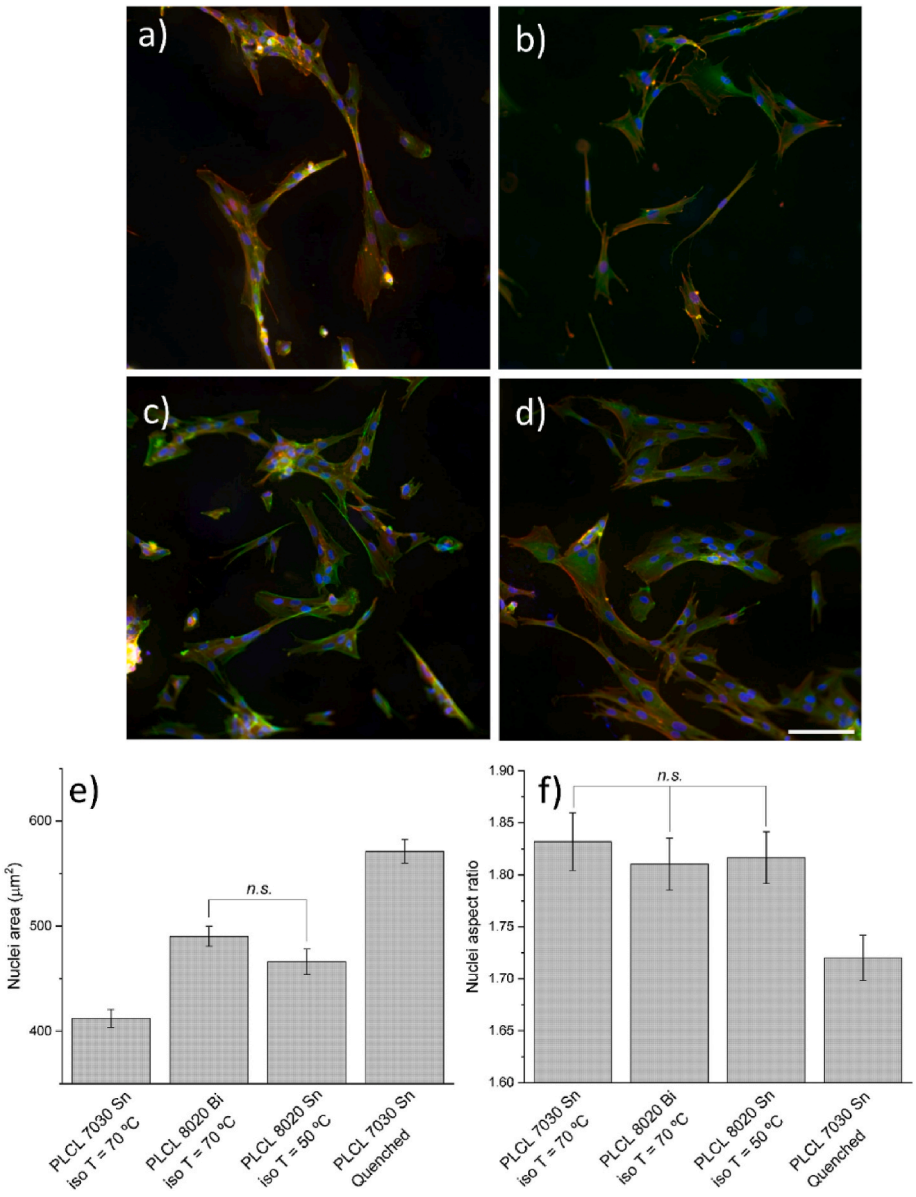

Fig. 5. Micrographs of MRC-5 cells seeded on a) PLCL 7030 Sn subjected to an isothermal treatment at 70 °C, b) PLCL 8020 Bi subjected to an isothermal treatment at 70 °C, c) PLCL 8020 Sn subjected to an isothermal treatment at 50 °C and d) PLCL 7030 Sn subjected to a rapid quenching from the melt. Blue: DAPI (Nuclei); Red: Rhodamine-Phalloidin (Actin filaments); Green: Vinculin (Focal adhesions); Scale bar: 100 μm. Quantification of nuclei area (e) and aspect ratio (f) (N = 250). Error bars represent the standard error of the mean. n. s. indicates that no significant differences exist between the highlighted samples ($p < 0.05$). (For interpretation of the references to colour in this figure legend, the reader is referred to the Web version of this article.)

(Table 2S). Immunostaining micrographs indicated that MRC-5 cells were able to firmly adhere to the surface of these three samples (Fig. 12S). Again, cells seeded on semicrystalline samples (i.e., PCL and PLLA_crystallized) showed a more elongated morphology, suggesting the importance of surface topography on cell interaction.

The surface topography influences several important aspects of cells, including adhesion, proliferation and differentiation and strongly depends on the studied cell type. The strategy described in the present study, that relies on adjusting the chain microstructure and thermal treatments to tune the surface topography of the samples, would allow us to adjust the surface biophysical properties of the materials to fit within the requirements of the intended use. For example, osteoblasts show a better proliferation in samples with increasing surface roughness, while fibroblast prefer smoother surfaces [39]. Controlling the surface topography also allows preserving the characteristic phenotype of primary cultures (e.g., chondrocytes), which is vital for regenerative strategies that rely on tissue engineering techniques [4,40]. More recently, the impact of surface topography on the foreign body response, which will eventually determine the success of the implanted material for its intended use, has attracted increasing attention [8,41]. Thus, considering the importance of surface topography on several aspects of the biomaterials, we expect to further study the impact of these biophysical parameters on neuroinflammatory processes in the future, by using our thermoplastic elastomers with controllable surface topography and texture.

4. Conclusions

In the present study, a plethora a polymeric films displaying a variety of surface topographies were developed by precisely controlling the chain microstructure of lactide and caprolactone-based copolymers. The composition of the copolymers defined the mechanical properties of the

resulting samples, which showed a plastic-like behaviour for those copolymers having 80 wt% of L-lactide and an elastomeric behaviour for those copolymers having 70 wt% of L-lactide. The selected catalyst ($SnOct_2$ vs. Ph_3Bi) determined the chain microstructure, resulting in a more random distribution of repetitive units when Ph_3Bi was used as a catalyst. This fact clearly determines the crystallization behaviour of the copolymers from the melt, which allowed us to obtain a wide variety of surface textures, ranging from smooth surfaces in the case of amorphous copolymers to rough surfaces in the case of copolymers having spherulitic or axialitic crystalline domains. In our preliminary *in vitro* study using human fibroblasts as model cells, we observed that cells interact differently depending on the surface biophysical properties of the films. This encourage us to further study the influence of surface topography and roughness derived from various crystallinity degrees and crystal morphologies on different cell processes, including inflammatory processes and foreign body responses.

Declaration of competing interest

The authors declare that they have no known competing financial interests or personal relationships that could have appeared to influence the work reported in this paper.

Data availability

Data will be made available on request.

Acknowledgments

This work has been funded by the Basque Government (GV/EJ) - Department of Education (GIC21/131 IT1766-22), grant PID2019-106236 GB-I00 funded by MCIN/AEI/10.13039/501100011033 and PID2022-139821OB-I00 funded by MCIN/AEI/10.13039/501100011033 and "ERDF A way of making Europe". C.B-Á. acknowledges the predoctoral grant funded by the UPV/EHU.

Appendix A. Supplementary data

Supplementary data to this article can be found online at https://doi.org/10.1016/j.polymertesting.2023.108220.

References

[1] F.J. O'Brien, Biomaterials & scaffolds for tissue engineering, Mater. Today 14 (2011) 88–95, https://doi.org/10.1016/S1369-7021(11)70058-X.
[2] B.P. Chan, K.W. Leong, Scaffolding in tissue engineering: general approaches and tissue-specific considerations, Eur. Spine J. 17 (2008) 467–479, https://doi.org/10.1007/s00586-008-0745-3.
[3] H. Ye, K. Zhang, D. Kai, Z. Li, X.J. Loh, Polyester elastomers for soft tissue engineering, Chem. Soc. Rev. 47 (2018) 4545–4580, https://doi.org/10.1039/C8CS00161H.
[4] E.C. Martínez, J.C.R. Hernández, M. Machado, J.F. Mano, J.L.G. Ribelles, M. M. Pradas, M.S. Sánchez, Human chondrocyte morphology, its dedifferentiation, and fibronectin conformation on different PLLA microtopographies, Tissue Eng. 14 (2008) 1751–1762, https://doi.org/10.1089/ten.tea.2007.0270.
[5] M.J. Dalby, S.J. Yarwood, M.O. Riehle, H.J.H. Johnstone, S. Affrossman, A.S. G. Curtis, Increasing fibroblast response to materials using nanotopography: morphological and genetic measurements of cell response to 13-nm-high polymer demixed islands, Exp. Cell Res. 276 (2002) 1–9, https://doi.org/10.1006/excr.2002.5498.
[6] Y. Polo, J. Luzuriaga, J. Iturri, I. Irastorza, J.L. Toca-Herrera, G. Ibarretxe, F. Unda, J.R. Sarasua, J.R. Pineda, A. Larrañaga, Nanostructured scaffolds based on bioresorbable polymers and graphene oxide induce the aligned migration and accelerate the neuronal differentiation of neural stem cells, Nanomedicine 31 (2021), 102314, https://doi.org/10.1016/j.nano.2020.102314.
[7] J. Luo, M. Walker, Y. Xiao, H. Donnelly, M.J. Dalby, M. Salmeron-Sanchez, The influence of nanotopography on cell behaviour through interactions with the extracellular matrix–a review, Bioact. Mater. (2021), https://doi.org/10.1016/j.bioactmat.2021.11.024.
[8] J.C. Doloff, O. Veiseh, R. de Mezerville, M. Sforza, T.A. Perry, J. Haupt, M. Jamiel, C. Chambers, A. Nash, S. Aghlara-Fotovat, J.L. Stelzel, S.J. Bauer, S.Y. Neshat, J. Hancock, N.A. Romero, Y.E. Hidalgo, I.M. Leiva, A.M. Munhoz, A. Bayat, B. M. Kinney, H.C. Hodges, R.N. Miranda, M.W. Clemens, R. Langer, The surface topography of silicone breast implants mediates the foreign body response in mice, rabbits and humans, Nat. Biomed. Eng. 5 (2021) 1115–1130, https://doi.org/10.1038/s41551-021-00739-4.
[9] E.S. Ereifej, C.S. Smith, S.M. Meade, K. Chen, H. Feng, J.R. Capadona, The neuroinflammatory response to nanopatterning parallel grooves into the surface structure of intracortical microelectrodes, Adv. Funct. Mater. 28 (2018), 1704420, https://doi.org/10.1002/adfm.201704420.
[10] C. Bello-Álvarez, A. Etxeberria, Y. Polo, J.R. Sarasua, E. Zuza, A. Larrañaga, Lactide and ethylene brassylate-based thermoplastic elastomers and their nanocomposites with carbon nanotubes: synthesis, mechanical properties and interaction with astrocytes, Polymers 14 (2022) 4656, https://doi.org/10.3390/polym14214656.
[11] J. Fernández, M. Montero, A. Etxeberria, J.R. Sarasua, Ethylene brassylate: searching for new comonomers that enhance the ductility and biodegradability of polylactides, Polym. Degrad. Stabil. 137 (2017) 23–34, https://doi.org/10.1016/j.polymdegradstab.2017.01.001.
[12] M. Malin, M. Hiljanen-Vainio, T. Karjalainen, J. Seppälä, Biodegradable lactone copolymers. II. Hydrolytic study of ε-caprolactone and lactide copolymers, J. Appl. Polym. Sci. 59 (1996) 1289–1298, https://doi.org/10.1002/(SICI)1097-4628(19960222)59:8<1289::AID-APP12>3.0.CO;2-1.
[13] J. Fernández, E. Meaurio, A. Chaos, A. Etxeberria, A. Alonso-Varona, J.R. Sarasua, Synthesis and characterization of poly (l-lactide/ε-caprolactone) statistical copolymers with well resolved chain microstructures, Polymer 54 (2013) 2621–2631, https://doi.org/10.1016/j.polymer.2013.03.009.
[14] Y. Wang, M. Xia, X. Kong, S. John Severtson, W.-J. Wang, Tailoring chain structures of l -lactide and ε-caprolactone copolyester macromonomers using rac -binaphthyl-diyl hydrogen phosphate-catalyzed ring-opening copolymerization with monomer addition strategy, RSC Adv. 7 (2017) 28661–28669, https://doi.org/10.1039/C7RA05531E.
[15] Z.Y. Wei, L. Liu, J. Gao, P. Wang, M. Qi, The copolymerization of l-lactide and ϵ-caprolactone using magnesium octoate as a catalyst, Chin. Chem. Lett. 19 (2008) 363–366, https://doi.org/10.1016/j.cclet.2008.01.004.
[16] R. Verónica Castillo, A.J. Müller, J.M. Raquez, P. Dubois, Crystallization Kinetics and Morphology of Biodegradable Double Crystalline PLLA-b-PCL Diblock Copolymers | Macromolecules, (n.d.). https://doi.org/10.1021/ma100201g.
[17] R.-M. Ho, P.-Y. Hsieh, W.-H. Tseng, C.-C. Lin, B.-H. Huang, B. Lotz, Crystallization-induced orientation for microstructures of poly(l-lactide)-b-poly(ε-caprolactone) diblock copolymers, Macromolecules 36 (2003) 9085–9092, https://doi.org/10.1021/ma0347868.
[18] H. Tsuji, Y. Tezuka, S.K. Saha, M. Suzuki, S. Itsuno, Spherulite growth of l-lactide copolymers: effects of tacticity and comonomers, Polymer 46 (2005) 4917–4927, https://doi.org/10.1016/j.polymer.2005.03.069.
[19] A. Pascual, H. Sardon, A. Veloso, F. Ruipérez, D. Mecerreyes, Organocatalyzed synthesis of aliphatic polyesters from ethylene brassylate: a cheap and renewable macrolactone, ACS Macro Lett. 3 (2014) 849–853, https://doi.org/10.1021/mz500401u.
[20] A. Sangroniz, L. Sangroniz, S. Hamzehlou, J. del Río, A. Santamaria, J.R. Sarasua, M. Iriarte, J.R. Leiza, A. Etxeberria, Lactide-caprolactone copolymers with tuneable barrier properties for packaging applications, Polymer 202 (2020), 122681, https://doi.org/10.1016/j.polymer.2020.122681.
[21] D.W. Grijpma, G.J. Zondervan, A.J. Pennings, High molecular weight copolymers of l-lactide and ε-caprolactone as biodegradable elastomeric implant materials, Polym. Bull. 25 (1991) 327–333, https://doi.org/10.1007/BF00316902.
[22] Y. Shen, K.J. Zhu, Z. Shen, K.-M. Yao, Synthesis and characterization of highly random copolymer of ε-caprolactone and D,L-lactide using rare earth catalyst, J. Polym. Sci. Polym. Chem. 34 (1996) 1799–1805, https://doi.org/10.1002/(SICI)1099-0518(19960715)34:9<1799::AID-POLA18>3.0.CO;2-1.
[23] I. Nifant'ev, P. Komarov, V. Ovchinnikova, A. Kiselev, M. Minyaev, P. Ivchenko, Comparative experimental and theoretical study of Mg, Al and Zn aryloxy complexes in copolymerization of cyclic esters: the role of the metal coordination in formation of random copolymers, Polymers 12 (2020) 2273, https://doi.org/10.3390/polym12102273.
[24] F. Li, S. Rastogi, D. Romano, Easy access to ultra-high molecular weight polylactones using a bismuth catalyst, J. Catal. 415 (2022) 123–133, https://doi.org/10.1016/j.jcat.2022.09.015.
[25] H.R. Kricheldorf, G. Behnken, G. Schwarz, P. Simon, M. Brinkmann, High molar mass poly(trimethylene carbonate) by Ph2BiOEt and Ph2BiBr-initiated ring-opening polymerizations, J. Macromol. Sci., Part A. 46 (2009) 353–359, https://doi.org/10.1080/10601320902724800.
[26] Z. Wei, C. Jin, Q. Xu, X. Leng, Y. Wang, Y. Li, Synthesis, microstructure and mechanical properties of partially biobased biodegradable poly(ethylene brassylate-co-ε-caprolactone) copolyesters, J. Mech. Behav. Biomed. Mater. 91 (2019) 255–265, https://doi.org/10.1016/j.jmbbm.2018.12.019.
[27] J. Fernández, A. Larrañaga, A. Etxeberria, J.R. Sarasua, Tensile behavior and dynamic mechanical analysis of novel poly(lactide/δ-valerolactone) statistical copolymers, J. Mech. Behav. Biomed. Mater. 35 (2014) 39–50, https://doi.org/10.1016/j.jmbbm.2014.03.013.
[28] J. Fernández, A. Etxeberria, J.R. Sarasua, Synthesis, structure and properties of poly(L-lactide-co–caprolactone) statistical copolymers, J. Mech. Behav. Biomed. Mater. 9 (2012) 100–112, https://doi.org/10.1016/j.jmbbm.2012.01.003.
[29] E. Pretsch, J. Seibl, W. Simon, Tables of Spectral Data for Structure Determination Organic Compounds, vol. 3, 2015, p. 626, 9783540124061., in: n.d.
[30] J.R. Sarasua, R.E. Prud'homme, M. Wisniewski, A. Le Borgne, N. Spassky, Crystallization and melting behavior of polylactides, Macromolecules 31 (1998) 3895–3905, https://doi.org/10.1021/ma971545p.
[31] J. Fernández, H. Amestoy, H. Sardon, M. Aguirre, A.L. Varga, J.-R. Sarasua, Effect of molecular weight on the physical properties of poly(ethylene brassylate)

homopolymers, J. Mech. Behav. Biomed. Mater. 64 (2016) 209–219, https://doi.org/10.1016/j.jmbbm.2016.07.031.
[32] K. Burg, Chapter 6 - poly(α-ester)s, in: S.G. Kumbar, C.T. Laurencin, M. Deng (Eds.), Natural and Synthetic Biomedical Polymers, Elsevier, Oxford, 2014, pp. 115–121, https://doi.org/10.1016/B978-0-12-396983-5.00006-5.
[33] J. Kasperczyk, M. Bero, Coordination polymerization of lactides, 4. The role of transesterification in the copolymerization of L,L-lactide and ε-caprolactone, Makromol. Chem. 194 (1993) 913–925, https://doi.org/10.1002/macp.1993.021940315.
[34] E. Lizundia, S. Petisco, J.R. Sarasua, Phase-structure and mechanical properties of isothermally melt-and cold-crystallized poly (L-lactide), J. Mech. Behav. Biomed. Mater. 17 (2013) 242–251, https://doi.org/10.1016/j.jmbbm.2012.09.006.
[35] E. Zuza, J.M. Ugartemendia, A. Lopez, E. Meaurio, A. Lejardi, J.-R. Sarasua, Glass transition behavior and dynamic fragility in polylactides containing mobile and rigid amorphous fractions, Polymer 49 (2008) 4427–4432, https://doi.org/10.1016/j.polymer.2008.08.012.
[36] J. Fernandez, A. Etxeberria, J.M. Ugartemendia, S. Petisco, J.R. Sarasua, Effects of chain microstructures on mechanical behavior and aging of a poly(L-lactide-co-ε-caprolactone) biomedical thermoplastic-elastomer, J. Mech. Behav. Biomed. Mater. 12 (2012) 29–38, https://doi.org/10.1016/j.jmbbm.2012.03.008.
[37] Y. Yuryev, P. Wood-Adams, M.-C. Heuzey, C. Dubois, J. Brisson, Crystallization of polylactide films: an atomic force microscopy study of the effects of temperature and blending, Polymer 49 (2008) 2306–2320, https://doi.org/10.1016/j.polymer.2008.02.023.
[38] E. Costa Martínez, J.L. Escobar Ivirico, I. Muñoz Criado, J.L. Gómez Ribelles, M. Monleón Pradas, M. Salmerón Sánchez, Effect of poly(L-lactide) surface topography on the morphology of in vitro cultured human articular chondrocytes, J. Mater. Sci. Mater. Med. 18 (2007) 1627–1632, https://doi.org/10.1007/s10856-007-3038-1.
[39] T.P. Kunzler, T. Drobek, M. Schuler, N.D. Spencer, Systematic study of osteoblast and fibroblast response to roughness by means of surface-morphology gradients, Biomaterials 28 (2007) 2175–2182, https://doi.org/10.1016/j.biomaterials.2007.01.019.
[40] E. Costa, C. González-García, J.L. Gómez Ribelles, M. Salmerón-Sánchez, Maintenance of chondrocyte phenotype during expansion on PLLA microtopographies, J. Tissue Eng. 9 (2018), https://doi.org/10.1177/2041731418789829.
[41] C. Vallejo-Giraldo, K. Krukiewicz, I. Calaresu, J. Zhu, M. Palma, M. Fernandez-Yague, B. McDowell, N. Peixoto, N. Farid, G. O'Connor, L. Ballerini, A. Pandit, M.J. P. Biggs, Attenuated glial reactivity on topographically functionalized poly(3,4-ethylenedioxythiophene):P-toluene sulfonate (PEDOT:PTS) neuroelectrodes fabricated by microimprint lithography, Small 14 (2018), e1800863, https://doi.org/10.1002/smll.201800863.